Probing nanoscale stress fields in Er^{3+}-doped optical fibres using their native luminescence

2004 J. Phys.: Condens. Matter 16 4907

(http://iopscience.iop.org/0953-8984/16/28/011)

INSTITUTE OF PHYSICS PUBLISHING JOURNAL OF PHYSICS: CONDENSED MATTER

J. Phys.: Condens. Matter **16** (2004) 4907–4920 PII: S0953-8984(04)74359-3

Probing nanoscale stress fields in Er^{3+}-doped optical fibres using their native luminescence

Andrea Leto and Giuseppe Pezzotti

Ceramic Physics Laboratory and Research Institute for Nanoscience, RIN, Kyoto Institute of Technology, Sakyo-ku, Matsugasaki, 606-8585 Kyoto, Japan

E-mail: pezzotti@ipc.kit.ac.jp

Received 4 January 2004
Published 2 July 2004
Online at stacks.iop.org/JPhysCM/16/4907
doi:10.1088/0953-8984/16/28/011

Abstract

Photon- and electron-stimulated luminescence assessments have been quantitatively used in assessing Er^{3+}-doped silica-glass fibre to obtain information about (i) diffusional processes taking place at the core/clad interface and (ii) residual stresses piled up (during fibre manufacturing) both in the clad and in the filamentary core. The refractive index of the core in an optical fibre was found to be affected by residual stress; therefore, information about the micro/nanoscopic stress/structure of the optical fibre device, which is obtained through piezo-spectroscopic assessments on the fibre section, has been routinely used for inspection before and after preform drawing. A calculation of the thermal contribution to residual stress and a comparison between experimental and theoretical results are also offered in the discussion section.

1. Introduction

Rare-earth fibre amplifiers have a unique ability to transmit optical signals over long distances with relatively low attenuation. Despite the straightforward physical principles on which the optical fibre technology has been built, several technological challenges and unsolved problems remain [1]. As one important technological condition for future developments, an improved microscopic control of both glass structure and residual stress at the core/clad interface is mandatory for minimizing signal loss. The ultimate interface control, both in terms of chemistry and local stress state, holds promise to improve system reliability and to produce fibres with specialty claddings of improved performance.

The native rare-earth elements allowing signal paths within the filamentary core of glass fibres are well known photo- and cathodoluminescence activators in numerous synthetic solids. The observed light emissions arise from electronic processes involving transitions from excited states to ground states of doubly and triply ionized rare-earth atoms. These transitions and the

details of their spectra have been extensively studied [2–4]. Spectra include both narrow-band and broad-band emissions. The positions (wavelength) of these transitions are not greatly influenced by the local crystal structure, that is, by the crystal field at the site of the trivalent rare-earth ion [5]. Wavelength shift of selected spectral bands from trivalent luminescent ions can be used for the determination of local stresses, provided that the selected band is stress sensitive and suitably sharp and intense to allow adequate fitting [6]. We have recently shown that stress assessments can be systematically performed in glasses and optical devices with a nanometre spatial resolution by exploiting the high spectral efficiency of selected rare-earth dopants [7, 8]. In this paper, we show a quantitative piezo-spectroscopic assessment of the luminescence spectrum of Er^{3+}-doped silica fibres. Then, a structural and residual stress analysis of the core/clad interface of this fibre is presented both in the fibre preform and in the final device configuration after drawing, with a spatial resolution spanning from the micrometre to the nanometre scale. The impact of stress to the fibre loss is also discussed to some extent. Photo- and cathodoluminescence techniques are shown to be very useful tools for the quantitative analysis of microscopic stresses in optical fibres in general, and for monitoring the complicated thermo-mechanical effects related to their manufacturing process.

2. Theoretical background

The refractive index of the core in an optical fibre is affected by the residual stresses piled up during fibre manufacturing, this phenomenon being usually referred to as the *stress-optic effect* [9]. The elastic stress contribution to the refractive index can be quantitatively characterized by tensorial stress-optical equations. However, for light propagating along a homogeneous and isotropic core of an optical fibre, the change in refractive index, Δn, in the radial direction due to residual stress can be expressed by the following linear relationship:

$$\Delta n = C\sigma_{\mathrm{h}}/3 \tag{1}$$

where C is the stress-optic coefficient (e.g., -4.2×10^{-12} Pa^{-1} for pure silica glass [10]) and σ_{h} is the average hydrostatic residual stress ($\sigma_{\mathrm{u}} = \sigma_{\mathrm{h}}/3 =$ uniaxial stress). Given the negative value of C for silica glass, it follows that a residual compressive stress (i.e., for convention with a negative sign) stored in the core of the fibre will produce an increase in the refractive index of the fibre core with respect to that of the clad. This can indeed be considered to be a positive contribution to the efficiency of the optical fibre because, according to the Snell law [11], the higher the refractive index of the core with respect to that of the clad, the lower the signal loss in the fibre. It follows that the manufacturing process of silica-based optical fibres has to be accurately designed to avoid piling up of residual tensile stresses within the fibre core.

Residual stresses in the optical fibre are mainly developed during the fibre drawing process and they may arise from the superposition of thermal and mechanical factors. Both for thermal and mechanical origin of residual stresses, the incorporation of doping elements within the core structure plays the main role. As a matter of fact, those dopants increase the thermal expansion coefficient of the core above that of the clad but, at the same time, they decrease the core viscosity below that of pure-silica clad. Positive residual stresses (i.e., tensile stresses) are usually developed in the core by thermal processes involved with fibre drawing. During drawing, when the temperature of the high-silica core becomes lower than its softening temperature, the clad structure is frozen in its final shape, while the doped-silica core is still soft, because its softening temperature is lower than that of the clad. With decreasing temperature, the core glass structure also loses its capacity for thermal rearrangement by diffusion, and residual tensile stresses pile up within the core due to its higher thermal expansion coefficient, as compared to the clad. In calculating the thermal contribution to residual stresses [12], it

can be assumed in a first approximation that the Young modulus, E, the Poisson ratio, ν, and the linear expansion coefficient, α, are independent of temperature. In addition, assuming the absence of shear stresses, the stress components, σ_r, σ_θ, and σ_z (in cylindrical coordinates r, θ, and z, as taken with their origin on the fibre long axis) will only depend on r. From elastic mechanics equations [12, 13], it can be shown that the residual thermally induced stresses in the core/clad structure can be expressed as

$$\sigma_r^{(c)} = A_c \tag{2}$$

$$\sigma_r^{(cl)} = A_{cl} + (B_{cl}/r^2) \tag{3}$$

$$\sigma_\theta^{(c)} = A_c \tag{4}$$

$$\sigma_\theta^{(cl)} = A_{cl} - (B_{cl}/r^2) \tag{5}$$

$$\sigma_z^{(c)} = C_c \tag{6}$$

$$\sigma_z^{(cl)} = C_{cl} \tag{7}$$

where A, B, and C are constants in the steady-state regime (i.e., after complete cooling down from the drawing process), and the subscripts (c) and (cl) represent core and clad respectively. The stress state has also to obey the following boundary conditions:

$$\sigma_r^{(c)} = \sigma_r^{(cl)} \qquad \text{for } r = R_c \tag{8}$$

$$\sigma_r^{(cl)} = 0 \qquad \text{for } r = R_{cl} \tag{9}$$

$$\sigma_z^{(c)} R_c^2 + \sigma_z^{(cl)}(R_{cl}^2 - R_c^2) = 0 \tag{10}$$

where R_c and R_{cl} are the radius of the core and that of the clad, respectively. The temperature difference, $(T_{RT}–T_0)$, between room temperature, T_{RT}, and the softening temperature, T_0, is the driving force which induces thermal stresses in the fibre as it cools. Consequently, the softening point would determine the range over which stress is introduced into the core/clad structure. The equation for the axial stress in the clad can be written as [14]

$$\sigma_z^{(cl)} = (\alpha_{cl} - \alpha_c)(T_{RT} - T_0^{(c)})E/(R_{cl}^2/R_c^2)(\nu - 1) \tag{11}$$

where α is the coefficient of thermal expansion. The axial stress in the core, $\sigma_z^{(c)}$, can then be found from the boundary condition (10), provided that the geometry of the fibre is known. The thermal stress in coaxial cylinders can be solved according to Poritsky's general method [15] (i.e., under the assumption that the core is limited to hydrostatic stress behaviour). The stresses in the core are taken to be hydrostatic, hence:

$$\sigma_r^{(c)} = \sigma_z^{(c)} = \sigma_\theta^{(c)}. \tag{12}$$

Therefore, we can calculate all the components of the elastic stress field in the core structure from equations (10)–(12), and the stress components in the core from equations (3), (5), (8), and (9). When $\alpha_{cl} < \alpha_c$, elastic hydrostatic tension should be piled up in the core because the core bonds to the clad and is confined by cold glass on the ends and clad along the cylindrical surface. However, there are two important technological factors, which can contribute to alter the stress field from the pure elastic one. Additional axial stresses may be developed in the clad upon cooling from a stress-free state above the softening point of the core. This additional residual stress is thus developed when the core is fluid and depends on the coefficient of thermal expansion and the bulk modulus of the core above its softening point [14]. This additional stress field may lead, in particular glasses, to non-negligible discrepancies with respect to calculated elastic values [14]; however, it is not known *a priori* whether or not its magnitude can be negligible in high-silica glass. Another contribution to the overall stress field in the core/clad fibre may arise from the larger viscosity of the clad material with respect to the filamentary core during drawing. This leads to compressive residual stresses within the Er^{3+}-doped core

embedded in high-silica clad. When the viscosity of the core is higher than that of the clad (as in the case of Er^{3+}-doped fibres), a negative stress (compression) is usually developed within the core by the mechanical drawing process. This mechanical stress is known to linearly increase with increasing drawing force [12]. Drawing of high-silica fibres is usually performed at a temperature near the softening point of the clad fibre, the fibre preform being normally pulled at relatively low rates ($5–30 \times 10^{-2}$ m s^{-1}). This low drawing rate may somewhat confine the magnitude of the mechanically induced residual stress stored in high-silica fibres. Our concern is with the actual residual stress field developed within the core/clad fibre both during preforming and the successive drawing process. For this purpose, a reliable experimental approach seems to be preferable, given the complex thermomechanical phenomena behind the manufacturing process of core/clad fibres. Therefore, the residual stress field in both core and clad structures will be first measured by piezo-spectroscopic techniques and then compared to elastic stress solutions, according to the above equations (2)–(12).

3. Experimental procedures

The investigated fibre preform consisted of a high-silica layer (diameter $2R_{cl} = 10$ mm) encompassing an Er-doped internal core (diameter $2R_c = 0.4$ mm) with 10 mol% Ge and an unknown (ppm) fraction of Al added as codopants. This preform was laboratory made (i.e., kindly provided by the University of Southampton). The Er^{3+}-doped/high-silica optical fibre was a core/clad structure from Mitsubishi Cable, Ltd. The core of the fibre (diameter $2R_c = 4.8$ μm) contained 560 ppm Er_2O_3, 500 ppm Al_2O_3, and 13.7 mol% GeO_2. The clad (diameter $2R_{cl} = 120$ μm) was a high-silica glass grade. However, the precise composition of the optical fibre, an early prototype, was covered by industrial secret, thus not available to the authors.

The photoluminescence spectroscopy procedure used in this study was similar to that previously described [16]; however, a brief description will also be given here. Fluorescence lines of Er/Ge substitutional impurities in silica glass were collected at room temperature. The sample surface was irradiated with an Ar^+ ion laser (wavelength of 488 nm, at 5 mW power, $\sim$1 μm spot size) in which an optical microscope was used to both focus the laser on the sample surface and to collect its scattered radiation. A triple monochromator (T64000, Jobin-Yvon/Horiba Group, Tokyo, Japan) equipped with a CCD detector was used to perform the analysis. A small bend bar was obtained by cutting the fibre preform in a plane perpendicular to its long axis and loaded in a three-point bending jig (equipped with a load cell of 100 N). The jig was then placed on to the microscope stage of the Raman spectroscopic apparatus. An automatic travelling stage, having a 0.1 μm maximum lateral displacement resolution, was used to direct the laser spot to the desired locations on the sample surface. An area $\sim$500 μm by $\sim$500 μm inside the Er^{3+}-doped core was selected, and the fluorescence spectra of this area were obtained by collecting individual spectra at a 1 μm by 1 μm gridlike array of points over this selected area. A schematic diagram of the cutting procedure of the bending bar from the fibre perform and of the loading jig are shown in figures 1(A) and (B), respectively. The scanning electron microscope (SEM) employed in this study was a new thermal filament type field emission gun (FEG) device with a lateral spatial resolution of 1.5 nm (JSM-6500F, JEOL, Tokyo, Japan). The microscope was mounted within a cut-out on an air-suspended optical table, thus eliminating vibration and aiding optical alignment. A high-sensitivity cathode luminescence detector unit (MP-32FE, Atago Bussan, Horiba Group, Tokyo, Japan) was employed for the collection of light upon reflection into an ellipsoidal mirror and transmission through an optical fibre. The emitted light spectrum was analysed using a triple monochromator equipped with a CCD camera. A new mapping device (PMT R943-02 Select, Atago Bussan,

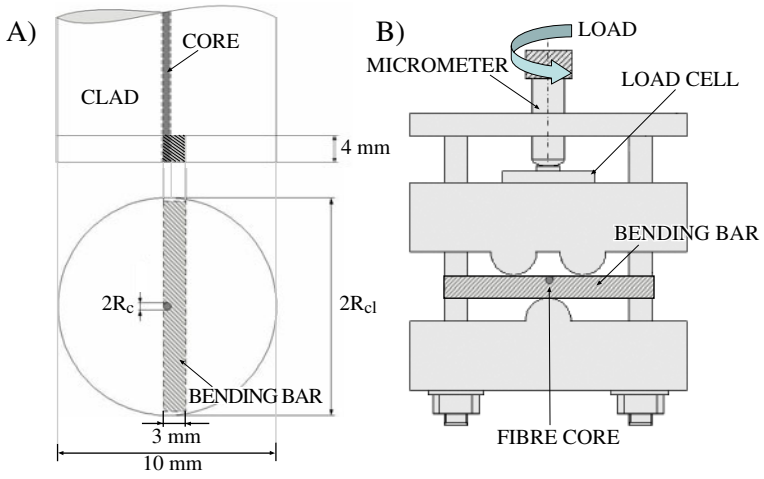

Figure 1. Schematic diagram of the experimental assessment adopted for piezo-spectroscopic calibrations by photoluminescence and electroluminescence peak-shift: (A) preparation of a bending specimen from the fibre preform; (B) three-point bending jig.

Horiba Group, Tokyo, Japan) and related software was developed which enabled us to collect with high spatial resolution, and automatically analyse, a large number of spectra. Spectra were analysed and then converted into stress maps using commercial software (Spectra Cal, Galactic Industries). The analysis of the spectra involved curve-fitting programs to estimate peak intensities and peak wavelength. Spectral wavelength shifts were obtained from the difference between the peak centres of stressed (residual and/or externally applied stresses) and unstressed conditions. The unstressed wavelength was estimated after extracting a small piece of the core structure from the clad. In the piezo-spectroscopic cathodoluminescence measurements, the strategy for obtaining very high spatial resolution was the same as that previously suggested by Warwick [17]: (i) using a low accelerating voltage (1.5 kV) to inject electrons into the surface with minimal lateral scattering (1.5 nm); (ii) using a small probe generated by a bright, field-emission source; (iii) detecting photons from pre-diffusion radiative recombination events. We were aided in this effort by the high efficiency of the luminescent Er^{3+} probe present in the fibre. A spectrum of good quality, suitable for precise mathematical fitting, could be collected within one second. Despite the occurrence of electron beam broadening, the highest spatial resolution achieved was better than 3 nm, as calculated according to the modified Grün equation [18]. A comprehensive discussion of the actual spatial resolution achievable in cathodoluminescence assessments has been recently given by Norman [19], therefore this topic will not be further addressed in this paper. Mechanical loading in the SEM was performed with a miniature bending-jig, according to the same procedure as described for the laser-excited photoluminescence assessments (see figure 1).

4. Results and discussion

4.1. Luminescence spectra and related piezo-spectroscopic calibrations

Typical photon- and electron-stimulated luminescence spectra are shown in figures 2(A)–(C), which were obtained from the fibre preform in the high-silica clad area and at the Er/Ge-doped core. A spectral doublet centred at 548 and 550 nm, due to the presence

Table 1. Results of piezo-spectroscopic calibrations for various photon (PL) and electron-stimulated luminescence (EL) bands, as detected in Er/Ge-doped optical devices.

Band (nm)	Measurement	(nm GPa^{-1})	(nm GPa^{-1})	Origin
410	CL	6.744	5.5×10^3	Dicoordinated Ge
460	CL	−6.529	1.37×10^3	Silica oxygen lack
548	PL	$<10^{-7}$	—	$^4S_{3/2}$ Er^{3+} transition
550	PL	−0.689	2.716×10^4	$^4S_{3/2}$ Er^{3+} transition
630	CL	−8.137	3.122×10^3	Silica oxygen excess

of Er^{3+} dopant, was clearly detected in the photoluminescence spectra recorded from the core (figure 2(A)). These peaks, which may arise from the $^4S_{3/2}$ electronic transition of the Er^{3+} dopant [4], are not the most intense luminescence bands of Er^{3+}-doped silica but were considered to be the most suitable for photo-stimulated piezo-spectroscopic assessments in the visible wavelength interval because of their relatively high sharpness. On the other hand, no suitable photoluminescence band could be collected from areas belonging to the high-silica clad structure. Figures 2(B) and (C) show the electron-stimulated luminescence spectra collected from core and clad areas, respectively, in the fibre preform. As seen, the spectrum in the core region appears to be rather complicated due to overlapping of four bands, two located at 410 and 650 nm and an additional two located at 460 and 630 nm. These latter two bands were reported to arise from lack and excess of oxygen in the silica structure, respectively [20]. In particular, the spectral band located at 460 nm was reported to be generated upon oxygen ion or γ-irradiation of silica glass, according to the formation of a species of peroxy radical (POR) bond of the type $O_3 = -Si–O–O^-$ ($^-$: unpaired electron) [20]. It should be noted that the most intense cathodoluminescence band located at 410 nm is due to dicoordinated Ge dopant [20]. These bands are different from the bands recorded for the photo-stimulated spectrum (see figure 2(A)).

Uniaxial stress, σ_u, was applied, as it develops upon loading a bar sample in a bending calibration jig. Accordingly, where luminescence peaks were available, their spectral shifts were evaluated both within the high-silica clad and the Er/Ge-doped core glass (see draft in figure 1). Given the relatively narrow stress range investigated, wavelength shifts, $\Delta\lambda$, of each spectral band (with respect to their respective unstressed wavelengths, λ_0) and uniaxial stresses, σ_u, could be related by a linear relationship, as follows:

$$\sigma_u = \Delta\lambda / \Pi_u \tag{13}$$

where Π_u is referred to as the piezo-spectroscopic coefficient for uniaxial stress. The average hydrostatic (three-dimensional) piezo-spectroscopic coefficient was taken as $\Pi_h = 3\Pi_u$, assuming a three-dimensionally isotropic structure for the glass fibre. Since residual (thermal) stresses resulting from sample processing were the object of our investigation, a stress-free (reference) wavelength, λ_0, had to be carefully selected. For this purpose, a map of luminescence spectra was collected within the sample from a small piece of core material cut from the clad, thus having zero residual and external stresses. The wavelength corresponding to the average spectrum of the map was taken as the reference wavelength, λ_0. A similar procedure was adopted for determining the λ_0 of the clad glass. Table 1 shows the results of piezo-spectroscopic calibrations with respect to the available bands belonging to both photo- and electron-stimulated luminescence spectra. The confidence of the measurements is also shown in terms of scattering of the piezo-spectroscopic coefficient, Π_u. Of the two photoluminescence Er^{3+} bands, the one located at lower wavelength was fairly insensitive to stress, while the Π_u value of the other one was of an appreciable value (see table 1) and similar to that measured

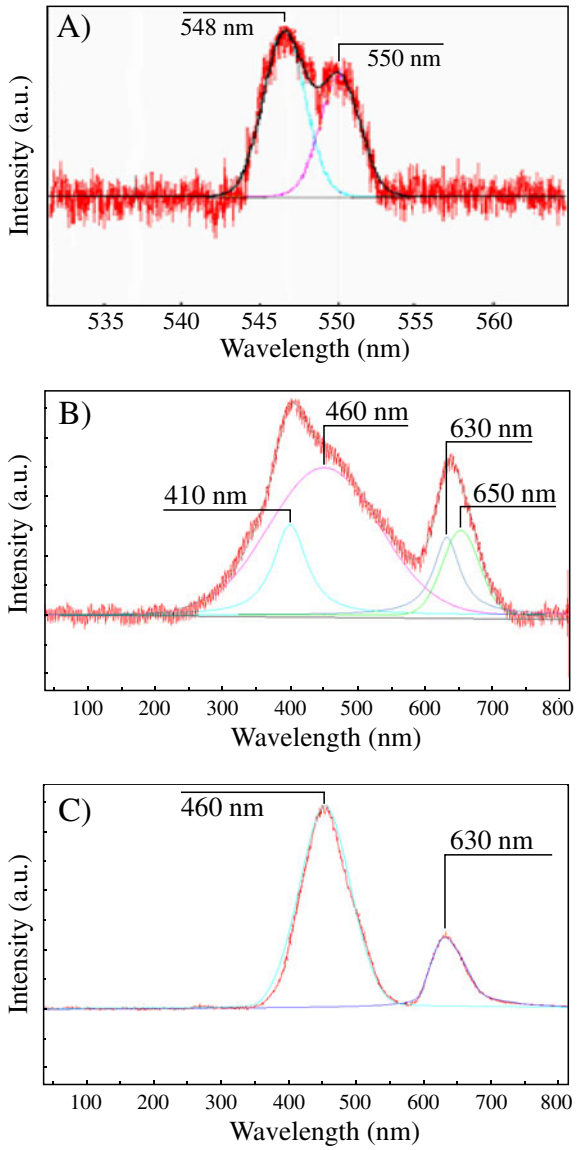

Figure 2. Luminescence bands and their respective deconvolution procedures: (A) photo-stimulated luminescence in the core; (B) electron-stimulated luminescence in the core; and (C) electron-stimulated luminescence in the clad.

in Sm^{3+}-doped alumino-silicate glass [7]. Four main cathodoluminescence bands (arising from Ge dopant and from silica defects) strongly overlapped in the core structure, which made necessary a preliminary deconvolution of the spectrum (as shown in figure 2(B)). Among those bands, a successful band-shift calibration could be obtained for the Ge band located at 410 nm. A fortunate circumstance for calibration arose from the rather high increase in relative intensity of the 410 nm band (i.e., with respect to the 460 nm band arising from silica defects) upon increasing the acceleration voltage of electron stimulation. The spectral shift of this band was sensitively and reliably related to stress. The 410 nm band was thus selected for residual stress

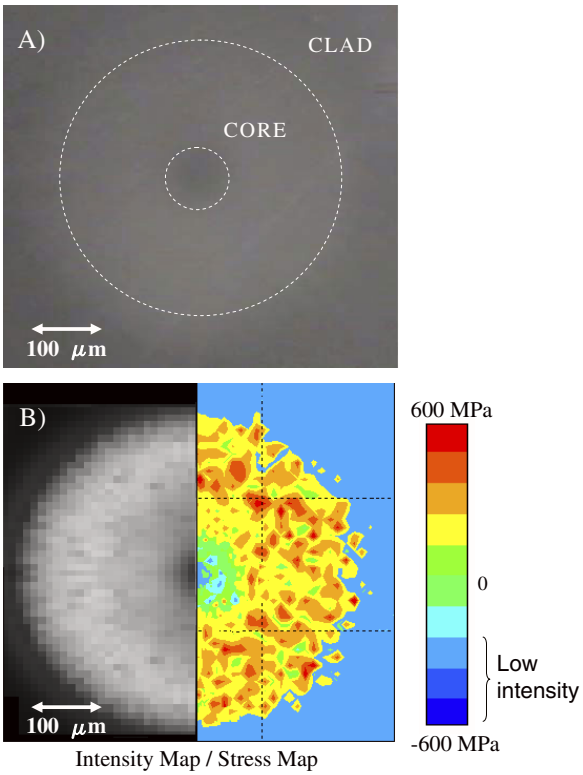

Figure 3. Optical image (A) of the core/clad area in the fibre preform and related intensity/residual stress map (B), as obtained from the photoluminescence shift of the 548 nm photo-stimulated Er^{3+} band (spatial resolution of 5 μm). Note the dark area at the centre of the core, due to the manufacturing process.

assessments within the fibre core. Unexpectedly, the two bands belonging to defect and excess oxygen in the high-silica clad both showed high sensitivity to stress, their spectral shift being of magnitude comparable with that of the 410 nm Er^{3+} band. In assessing residual stresses in the clad structure, the oxygen-lack band centred at 460 nm ($\Pi_u = -6.529$ nm GPa^{-1}) was selected because of its higher intensity.

4.2. Experimental residual stress field in preform and fibre core/clad structures

Sections of the core/clad preform were mapped with respect to both luminescence band intensity and spectral shift. From the map of spectral shift, a residual stress map was calculated according to equation (13) and the $\Pi_h = 3\Pi_u$ values from table 1. Figure 3 shows an optical image (A), a band intensity map and a residual stress map (B), as collected in the preform core using the photoluminescence Er band located at 548 nm. The spatial resolution of this stress measurement was 5 μm. The map in (B) clearly indicates a region of relatively high tensile stress that corresponds with the core area, whilst in the clad region the Er band was too low and the stress field was almost undetectable, except for a small compressive-stress region close to the core/clad interface. A region of low intensity and moderate compressive stress was also noticed in a symmetric region of about 100 μm in diameter at the core centre. This characteristic is related to the manufacturing process of the core, and it may indicate

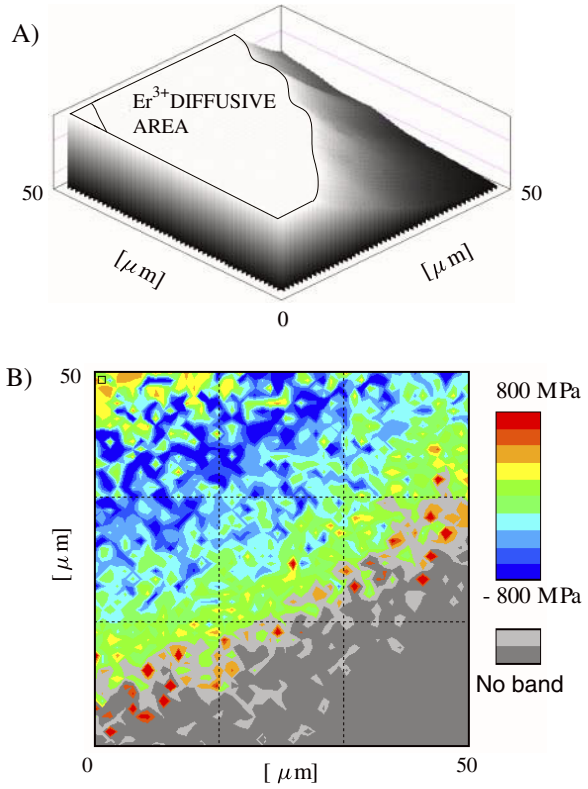

Figure 4. Photoluminescence intensity map (A) and stress map (B) as collected in the neighbourhood of the core/clad interface in the fibre perform (spatial resolution of 1 μm). The monitored zone in this experiment represents an area in which significant diffusion of Er^{3+} ions has occurred from the core towards the clad during manufacturing.

that the core has been processed according to a porous layer deposition procedure [1]. The maximum tensile stress recorded with the spatial resolution of 5 μm in the core region was about 600 MPa. Interestingly, a stress distribution was revealed to exist with a micrometre scale, which was attributed to the existence of microcracks within the core structure. This interpretation was supported by SEM observation in the core structure, as shown in the inset in figure 5. Although, as mentioned before, the 548 nm Er band was not detectable in the clad area, the stress at the core/clad interface could be measured by virtue of a certain number of Er ions which diffused during processing from the core area towards the clad. Figure 4 shows a photoluminescence band-intensity and a stress map recorded from an area close to the core/clad interface. In this further measurement, the spatial resolution was improved to 1 μm. From the intensity map (figure 4(A)), it is seen that the Er diffusion path extended for about 50 μm from the core towards the clad. This result is similar to the diffusion of Ge ions recorded in a previous study of optical fibres by cathodoluminescence [8]. Within this intermediate diffusive region compressive stress was developed (see figure 4(B)), which counterbalances the residual tensile stress developed in the core. Interestingly, the maximum stress magnitude recorded with the spatial resolution of 1 μm was 800 MPa, namely about 30% higher than that recorded with a probe of 5 μm. This suggests that the actual magnitude of residual stress depends on the configuration of the laser probe adopted, the higher the lateral resolution of the probe the closer the measured value to the surface stress field at the core/clad

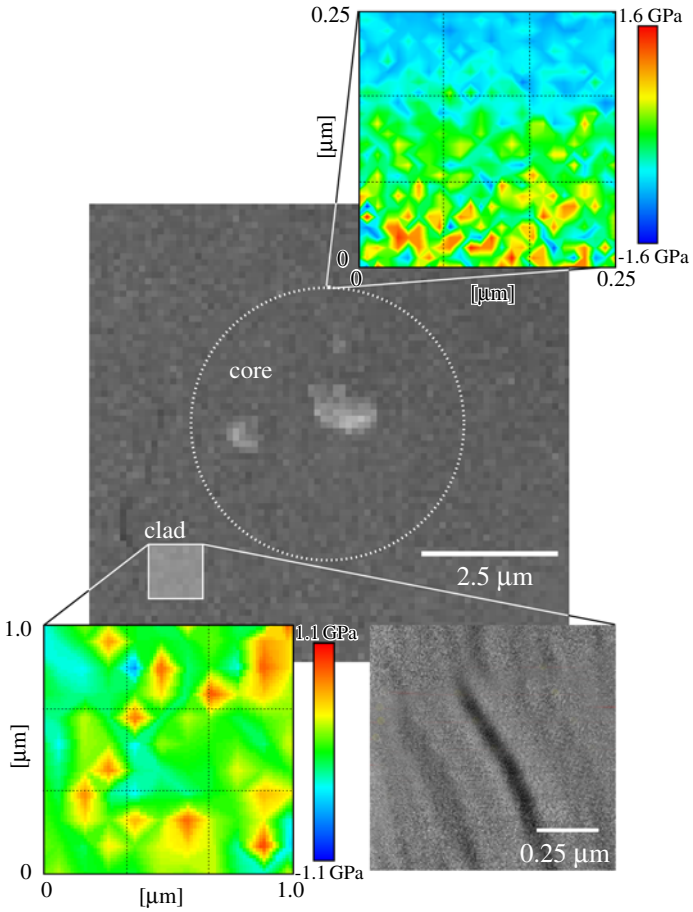

Figure 5. Scanning electron micrograph of the core area in the Er/Ge-doped core/clad fibre device. The core area was only about 5 μm in diameter. Related stress maps at the core/clad interface and in the clad area were obtained from the shift of the 410 and 630 nm cathodoluminescence bands, respectively (see figures 2(B) and (C), and table 1), with a (nominal) spatial resolution of 1.5 nm. Note the GPa stress intensification at the core/clad interface.

interface. The stress-field trend at the core/clad interface was in qualitative agreement with the elastic residual stress field calculated according to equations (2)–(12), as will be discussed in the forthcoming section.

After drawing the preform, the final configuration of the fibre consists of a central core cylinder of about 5 μm in diameter, embedded into a clad structure of about 120 μm in diameter. Given this microscopic configuration, an accurate stress measurement at the core/clad interface may require a nanometric spatial resolution, which can only be attained by means of electron-stimulated luminescence measurements. Figure 5 illustrates the results of field emission electron microscopy observation and piezo-spectroscopic nanostress analysis by cathodoluminescence for two selected areas at the core/clad interface and within the clad structure (i.e., far away from the interface) respectively. In this case, the acceleration voltage was set at 1 keV and the electron beam was focused to the maximum resolution of the microscope (1.5 nm). However, due to beam broadening, the maximum spatial resolution achieved was estimated to be about 3 nm, as calculated according to the Grün equation [17].

The 410 nm Ge band and the 460 nm oxygen-lack silica band were used for the core and the clad, respectively. When evaluated at a nanometre scale, local stresses were clearly higher (GPa level) than the average stresses measured with a micrometre resolution (e.g., using photoluminescence peak-shift), but their distribution was rather inhomogeneous. The arithmetical average of nanostress values calculated over a square micrometre area resulted in a value very close to that measured in the same area using a micrometre-size laser excitation in a confocal configuration. The detected inhomogeneous (micellar) structure was similar to that observed in a previous work on Sm^{3+}-doped glass samples [7]. From a general point of view, the way nanometre-scale stresses distribute within the glass structure may prove either the presence of nanocracks or the coexistence of strong and weak interpenetrating networks, with the attendant appearance of cohesive molecular groupings which mutually interact via the weak network while being internally bound throughout the strong. This feature has been discussed in some detail in a previous paper [7]. The average surface residual stress field in the clad structure was compressive of a very low magnitude (about -2 MPa), despite the locations of high tensile stress, which were observed on a sub-micrometric scale. On such a scale, local tensile stress accumulation may be due to the presence of small cracks, which were indeed observed within the clad structure of the fibre by high-resolution SEM (see inset in figure 5). These micro/nanomechanics characterizations suggest a significant impact of the residual stress field at the core/clad interface on the optical performance of the fibre device, according to equation (1). It should be noted that, given the local impact of stress on signal loss, residual stress intensification at the core/clad interface will practically involve a higher signal loss as compared to that predictable from a residual stress value averaged over all the core region (i.e., calculated from elastic mechanics theory or experimentally collected with a lower spatial resolution).

4.3. Comparison between experimental and theoretical stress fields

In an attempt to obtain a more comprehensive view of the residual stress field, a plot of the experimental hydrostatic stress, σ_h, was made and compared to the elastic stress field calculated through equations (2)–(12) (figure 6). Calculations were made taking the coefficients of thermal expansion of high silica and Er^{3+}-doped silica as $\alpha_{cl} = 0.7 \times 10^{-6}$ K^{-1} and $\alpha_c = 1.7 \times 10^{-6}$ K^{-1}, respectively. The stress-freezing interval of temperature was taken as $T_0^{(c)} - T_{RT} = 952$ K. The Young modulus, E, and the Poisson ratio, ν, for the clad glass were taken as 75 GPa and 0.18, respectively [21, 22]. The elastic stress field only depends on the ratio R_c/R_{cl}, and thus it was the same for both preform and fibre. The experimental σ_h values were calculated by averaging the values collected on each circle of radius r in the preform and plotted as a function of the ratio r/R_{cl}. One important feature in this plot is the existence of a tensile stress remarkably higher than that predicted by elastic calculations. In addition, the location of maximum stress within the core was detected at about $r/R_{cl} = 0.03$, thus away from the exact location of the core/clad interface ($r/R_{cl} = 0.04$). On the other hand, the average hydrostatic stress in the core showed very close tensile values when measured by photo- and electron-stimulated luminescence piezo-spectroscopy, which can be interpreted as evidence in support of the reliability of our experimental assessments. The hydrostatic stress value approached zero drastically as it reached the interface, and it became slightly negative within the clad area near the core/clad interface, before approaching zero. Compressive residual stresses were also stored at the centre of the core area, which could not be predicted by theoretical computations because in such computations the core structure was assumed to be of the same composition as the rest of the core. The present piezo-spectroscopic assessments seem to reliably evaluate the actual magnitude of the hydrostatic stress value,

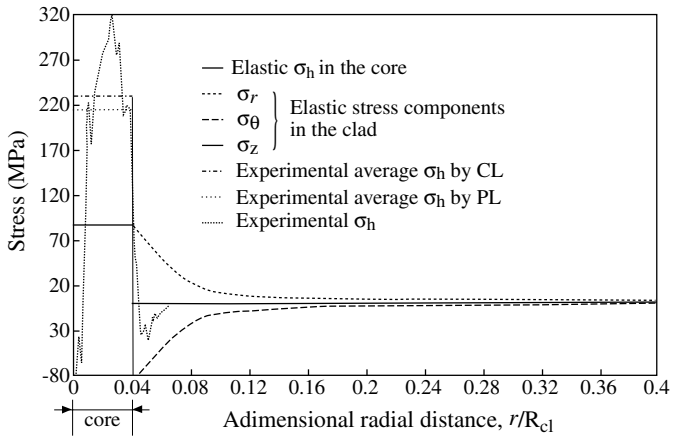

Figure 6. Plot of theoretically computed (elastic) residual stresses (i.e., according to equations (2)–(12)) and stresses experimentally measured by piezo-spectroscopic techniques. The abbreviations PL and CL refer to photoluminescence and cathodoluminescence methods, respectively.

$\sigma_{\mathrm{h}}^{(\mathrm{cl})} = \sigma_z^{(\mathrm{cl})} + \sigma_r^{(\mathrm{cl})} + \sigma_\theta^{(\mathrm{cl})}$, within the clad area, as seen from the good agreement between the low compressive stress either measured or calculated in the clad, away from the interface. Unfortunately, at the present stage of development of the piezo-spectroscopic technique, it is not possible to single out the individual components of the stress field and compare them to the respective calculated values. From a general perspective, however, it seems that just taking into account the difference between the coefficients of thermal expansion between core and clad does not give an highly accurate description of the actual residual stress state. It is possible that computational procedures underestimated the residual stress field because of neglecting additional sources of residual stress in the actual device. We have mentioned in section 2 the possible existence of a compressive stress component, which can be developed within the core due to a higher viscosity of the clad with respect to the core [12]. However, this seems not to be the case here because a compressive stress should reduce the stress field to a value lower than that calculated by purely elastic equations. On the other hand, additional tensile stress field may originate during cooling above the softening point of the core, when the core is still in a fluid state. Krohn [12] has discussed in some detail this phenomenon, showing that it may be the origin of discrepancy between calculated stress values and values measured by photoelasticity methods in the clad. The coefficient of expansion above the glass transition is approximately two to three times that below the transition, therefore large residual stresses may develop even for relatively low differences in softening temperature between core and clad. The present experiments also revealed that remarkable tensile stress intensification arose from the presence of micro/nanocracks within both core and clad. It should be noted that theoretical calculations can be refined and improved but the above facts, coupled with the occurrence of significant diffusion of Er^{3+} from the core volume towards the clad, will always make the residual stress field in fibre devices unpredictable to a large extent and call for systematic experimental assessments.

5. Conclusion

A piezo-spectroscopy technique, using the native luminescence of Er/Ge-doped optical fibres, was employed to probe the micro/nanoscopic residual stress field stored in the core/clad structure. Both photo- and electron-stimulated luminescence was used, in order to assess

the residual stress field from a micrometre to a nanometre scale. The correlation coefficient between stress and wavelength-shift of characteristic luminescence bands from the Er and Ge dopant in glass was systematically evaluated by an elastic (bending) calibration approach. In addition, two cathodoluminescence bands, peculiar to oxygen-related defects in silica, showed high stress sensitivity and were suitable for residual stress assessments in the high-silica clad. A linear correlation was obtained between peak frequency shift and external stress for suitable bands with a relatively high reliability, despite the glassy nature of the device. Residual stress distributions were measured both within the core and at the core/clad interface from the clad side, by exploiting the existence of a diffusion path for Er or Ge ions beyond the core/clad interface. From a general perspective, qualitative agreement was found between the measured and calculated residual stress fields. However, some important details in the experimental results differed from the calculations:

(i) a shift from the core/clad interface toward the core centre in the location of the maximum tensile stress, which was probably related to the presence of a compressive stress field at the core centre induced during core manufacturing, and
(ii) the magnitude of the hydrostatic tensile stress within the core volume was about four times larger than that obtained from elastic calculations of thermally induced residual stress, suggesting that a significant fraction of the residual stress field was stored in the device at temperatures above the softening temperature of the high-silica clad.

This study confirms the importance of experimental stress analyses as a counterpart of computational procedures for understanding the impact of residual stresses on the optical performance and in developing new manufacturing processes for optical devices. In addition, piezo-spectroscopic methods, applied from both photo- and electron-stimulated luminescence, may provide a useful tool for stress characterizations, complementary to photoelasticity and with the potential for the achievement of very high spatial resolutions.

Acknowledgments

The authors wish to acknowledge Professor O Sbaizero for his valuable contribution in discussing residual stresses, and Professors K Tanaka and S Tanabe for providing the investigated devices and for useful discussions.

References

[1] Simpson J R 1993 *Rare Earth Doped Fiber Lasers and Amplifiers* ed M J F Digonnet (New York: Dekker) pp 1–18
[2] Wybourne B G 1965 *Spectroscopic Properties of Rare Earths* (New York: Wiley–Interscience)
[3] Hufner S 1978 *Optical Spectra of Transparent Rare-Earth Compounds* (New York: Academic)
[4] Miniscalco W J 1993 *Rare Earth Doped Fiber Lasers and Amplifiers* ed M J F Digonnet (New York: Dekker) pp 19–133
[5] Dieke G H 1968 *Spectra and Energy Levels of Rare Earth Ions in Crystals* (New York: Wiley–Interscience)
[6] Forman R A *et al* 1972 *Science* **176** 284
[7] Pezzotti G 2003 *Microsc. Anal.* **33** 5
[8] Pezzotti G *et al* 2003 *J. Phys.: Condens. Matter* **15** 7687
[9] Aben H and Guillemet C 1993 *Photoelasticity of Glass* (New York: Springer)
[10] Primak W and Post D 1989 *J. Appl. Phys.* **30** 779
[11] Born M and Wolf E 1965 *Principles of Optics* (New York: Pergamon)
[12] Paek U C and Kurkjian C R 1975 *J. Am. Ceram. Soc.* **58** 330
[13] Krohn D A 1970 *J. Am. Ceram. Soc.* **53** 505
[14] Krohn D A and Cooper A R 1969 *J. Am. Ceram. Soc.* **52** 661

[15] Poritsky H 1934 *Physics* **5** 406
[16] Pezzotti G 1999 *J. Raman Spectrosc.* **30** 867
[17] Warwick C A 1991 *Inst. Phys. Conf. Ser.* **10** 681
[18] Everhart T E and Hoff P H 1971 *J. Appl. Phys.* **42** 5837
[19] Norman C E 2002 *Microsc. Anal.* **26** 5
[20] Skuja L 1998 *J. Non-Cryst. Solids* **239** 16
[21] Sakurai Y and Nagasawa K 2000 *J. Appl. Phys.* **88** 168
[22] Bansal N P and Doremus R H 1986 *Handbook of Glass Properties* (New York: Academic)